

Article

The Influence of Groundwater on the Sliding and Deposition Behaviors of Cataclinal Slopes

Cheng-Hsueh Weng ¹, Ming-Lang Lin ¹, Chia-Ming Lo ^{2,*} and Hsi-Hung Lin ^{1,3}

¹ Department of Civil Engineering, National Taiwan University, Taipei City 10617, Taiwan;

ppb428@gmail.com (C.-H.W.); mlin@ntu.edu.tw (M.-L.L.); hsihong.lin@msa.hinet.net (H.-H.L.)

² Department of Civil and Disaster Prevention Engineering, National United University, Miaoli City 36003, Taiwan

³ Central Geological Survey, MOEA, New Taipei City 23567, Taiwan

* Correspondence: cmlo@nuu.edu.tw or ppb428@yahoo.com.tw; Tel.: +886-37-382-365

Received: 27 June 2018; Accepted: 23 August 2018; Published: 3 September 2018



Abstract: In 2015, Typhoon Soudelor caused a number of slopes to collapse in Wulai District of New Taipei City. One of these landslides took place in the village of Zhongzhi and involved atypical cataclinal slope failure with a rock–soil interface. The remaining rock in the slope and the rock that originally covered it contained vertical joints, so groundwater could have flowed through the joints and influenced landslide behavior. However, few existing studies have examined the influence of upward groundwater flow on slope stability. To fill this gap, this study used physical tests and discrete element method software to conduct relevant investigations. We first conducted tests using the ground water flow and cataclinal slope simulator, in which water can flow out of holes in the platform to simulate upward-seeping groundwater. We used gypsum boards or rhombus-shaped grinding stones to simulate rock with vertical joints and round grinding stones mixed in paste to simulate cohesive regolith. The objective of the tests was to understand the influence of water flow on the landslide behavior of the specimens and the connections between movement behavior and the sequence of sliding between different materials during the landslide. We then reproduced the physical tests using discrete element method software PFC3D (Particle Flow Code 3D Version 4.0 by Itasca, Minneapolis, MN, USA) to display the influence of water flow on specimens, including the weakening of bond strength, decreasing coefficient of friction between particles, and the application of seepage force, as well as uplift and lateral forces caused by water pressure. This process gave us an understanding of the influence of different groundwater conditions on landslide behavior, which facilitates the study of landslide mechanisms and movement behavior. Finally, we applied the water flow influence settings to simulate and examine the Zhongzhi landslide process. Compared to methods that simply reduce the friction coefficients to trigger landslides, our numerical simulation was closer to reality in that in this case a rising water table triggered the landslide.

Keywords: cataclinal slope; groundwater; rock–soil interface; ground water flow and cataclinal slope simulator; discrete element method

1. Introduction

This study mainly focuses on the groundwater-caused sliding and deposition behaviors of cataclinal slopes. A cataclinal slope (also known as a dip slope) is a geomorphological topographic surface which dips in the same direction, and often by the same amount, as the true dip or apparent dip of the underlying strata. A cataclinal slope is often prone to translational slide, that typically takes place along structural features such as a bedding plane or the interface between resistant bedrock and weaker overlying material. The failure surfaces are usually structural discontinuities such as bedding planes, joints, faults, or the interface between bedrock and an overlying layer of weathered rock.

Between 6 and 9 August 2015, Typhoon Soudelor hit Taiwan and brought with it heavy rains. During the typhoon, the Fushan weather station measured a total accumulated rainfall of 792 mm. While this was not a record amount of rainfall for the area, the maximum hourly rainfall, three-hourly rainfall, six-hourly rainfall, and 12-hourly rainfall values reached 95 mm, 253 mm, 442 mm, and 655 mm, respectively. Such rains were not only more intense than those measured from other typhoon events; the frequency was also greater than that seen in events over the last 200 years. Typhoon Soudelor was therefore unprecedented in terms of short-duration, high-intensity rainfall [1]. It caused multiple landslides in the Wulai District of New Taipei City, including the landslide that took place in the hills of the village of Zhongzhi (hereinafter referred to as the Zhongzhi landslide), which was deemed to have been caused by debris sliding in preliminary investigations.

After the landslide, a cataclinal rock slope (hereinafter referred to as the cataclinal slope, Figure 1) and the rock that was originally covering it (hereinafter referred to as the jointed rock mass) was exposed in the middle section of the landslide area, both displaying joints with high inclination angles. Even in conditions with no rain, groundwater could be observed seeping out from the joints of the rock slope surface. It was therefore speculated that during heavy rain, the groundwater could seep upwards via the joints. Thus, in addition to rainfall infiltrating the surface and influencing the regolith during the torrential rains of Typhoon Soudelor, groundwater may also have seeped upwards via the joints, thereby raising the water table and weakening the regolith above. The groundwater in the cracks would also have applied an uplift force to the rock and undermined the stability of the weak stratum and rock–soil interface [2]. Thus, the influence of groundwater on slope stability and landslide behavior is also worthy of consideration.

In the Zhongzhi landslide during Typhoon Soudelor, the initial sliding surface may have originated from within the regolith or directly within the weak surface. However, it is difficult to grasp the entire process of the landslide solely from post-disaster investigation. To determine how such groundwater conditions influence the location of the initial sliding surface in cataclinal slopes, we simplified the profile of the Zhongzhi cataclinal slope and performed simulations with a physical model and a digital model. The objectives were to investigate: (1) the weakening effect of groundwater and the influence of the water pressure on slope failure behavior, (2) the influence of water flow on specimen landslide behavior, and (3) the sliding process of the Zhongzhi landslide. The methodology adopted can also provide reference for future related studies. Unlike in previous studies where physical modeling was conducted considering sliding mechanisms, we used a field-based approach to simplify the groundwater conditions in designing a physically-based model for cataclinal slopes. This physical model could be used to adjust parameters of the numerical model. This physical model could also be used to enrich analysis of the characteristics that lead from instability to deformation and sliding in cataclinal slopes by the influence of groundwater. The study implemented the water pressure model in PFC3D to simulate the slope deformation, failure, slide, and deposits for cataclinal slopes by the influence of groundwater. Our objective was to recreate the sliding behavior of a cataclinal slope in order to formulate predictions of landslide behavior and determine the landslide potential of such slopes. The selection of parameters for numerical simulation using the full-scale model was guided by preliminary physical model tests using a simplified physical model designed to identify the appropriate microscopic parameters of deformation and sliding behavior on cataclinal slopes. This approach could serve as reference for the PFC3D simulation of other cataclinal slopes.

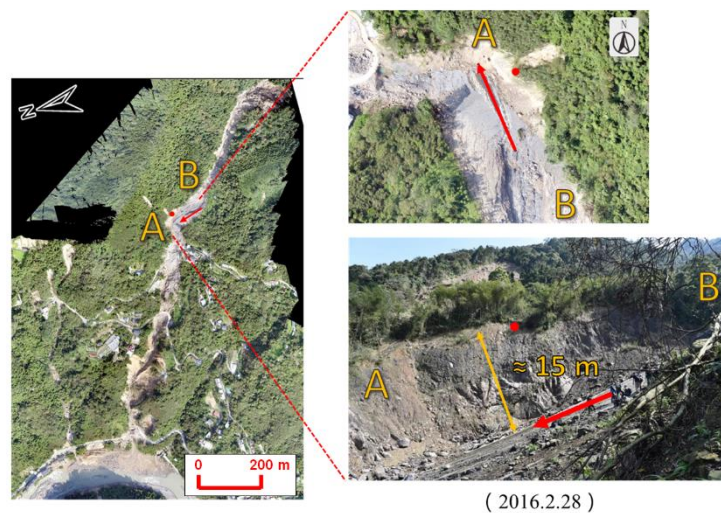


Figure 1. Location of the Zhongzhi landslide and the cataclinal slope [3].

2. Methodology

This study examined the cataclinal slope of the Zhongzhi landslide. We referred to the investigation conducted by [4] following Typhoon Soudelor and conducted our own field investigation to construct a conceptual model of the cataclinal slope. The onsite geological conditions were simplified, and the ground water flow and cataclinal slope simulator was used to perform a qualitative physical test. We attempted to display the slope failure under the influence of water flow in the discrete element method software Particle Flow Code (PFC) (Particle Flow Code 3D Version 4.0 by Itasca, Minneapolis, MN, USA) and reproduce the physical test. Finally, we applied it to the simulation of the full-scale real case to dissect the sliding process.

2.1. Field Investigation and Geological Condition

To examine the landslide mechanisms, we conducted a field investigation to construct a conceptual model. According to the 1:50,000 scale geological map compiled by the Central Geological Survey (Figure 2), the landslide area belongs to the Kankou Formation, the lithology of which includes argillite or sandy argillite occasionally interlaced with thin layers of sandstone. The Zhongzhi landslide took place on the slope of the northwestern wing of the Chaitianshan anticline. Both the strata and the slope roughly face northwest at approximately the same dip angle. Thus, this area forms a cataclinal slope. In terms of geological structure, the study area is located on the northwestern side of the Chaitianshan anticline. Inter-layer shear zones can also be found in the stratum, accompanied by small-scale faults and sporadic fracture zones; the rock mass close to the anticline is very broken, and the rock mass is often distorted (local areas can be found to be folded), deformed, or fragmented, causing the debris to collapse. In addition, debris slide and debris flow is frequent, so it is a critical geological structure in the study area. With the cataclinal slope as the divide, the strata exposed uphill of the landslide area contains whole and fragmented rock, while the slopes downhill of the cataclinal slope are mostly covered by colluvium, all the way to the area near Provincial Highway No. 9A, where the bedrock is exposed again.

After the landslide, we observed water seeping out from the strike joints in the cataclinal slope. This is evidence of groundwater emerging out of slope along joints (Figure 3). This is a classic mode of slope failure. Based on the exposed cliff surface, we can assume that the cataclinal slope was originally covered by sandy argillite with high-angle cracks and the regolith above it, as shown in Figure 3. The sliding in the landslide during Typhoon Soudelor may have taken place directly at the interface between the weathered rock mass and the bed rock or have arisen from failure in the regolith which then triggered the sliding of the rock mass. To confirm this, we constructed a conceptual model

(Figure 3) and conducted simulations using a physical model and a small-scale digital model. This enabled us to study the weakening effect of groundwater and the influence of the water pressure on slope failure behavior and understand the influence of water flow on specimen landslide behavior and the order in which sliding between different materials takes place during landslides.

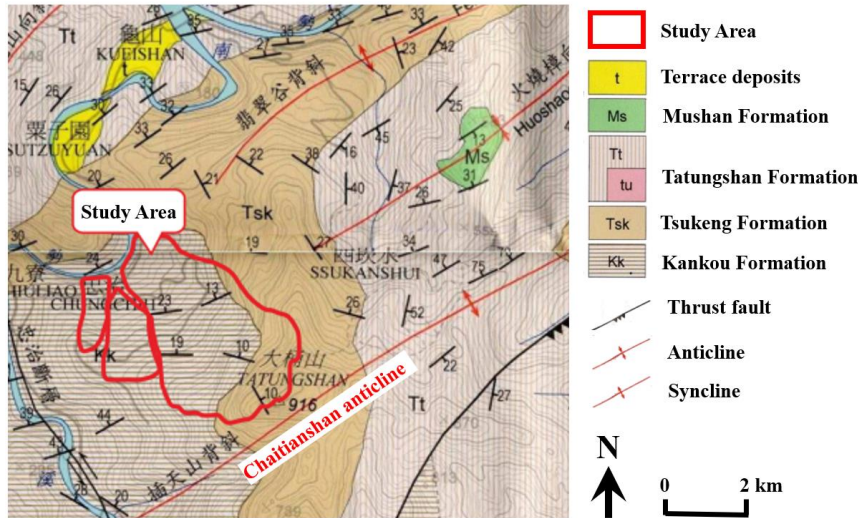


Figure 2. A 1:50,000 scale geological map of the study area.

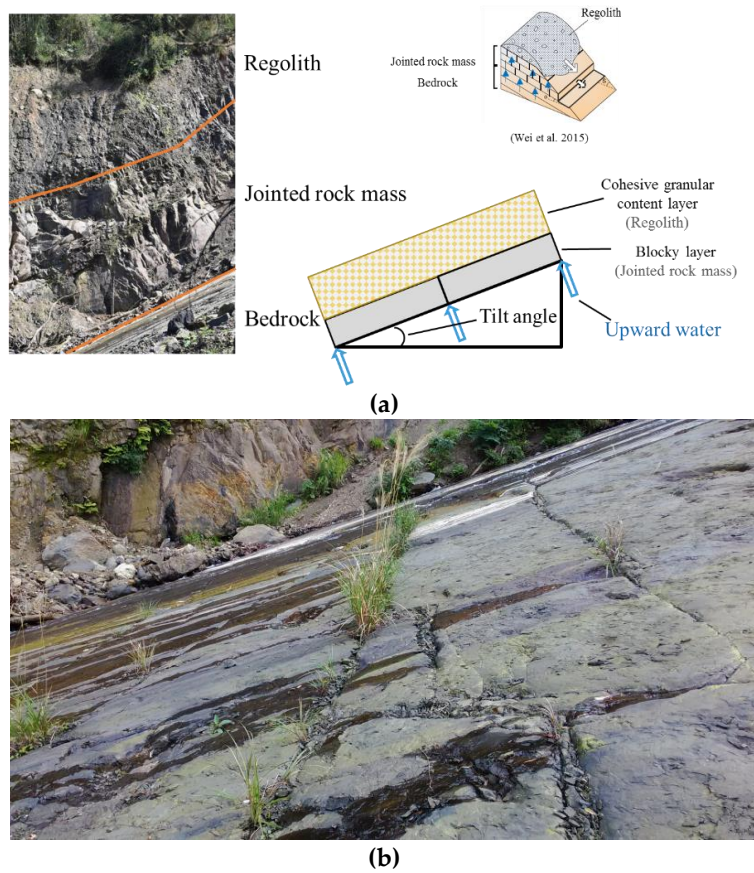


Figure 3. Profile and conceptual model of cataclinal slope (a) and groundwater emerging out of slope surface along joints (b).

2.2. Physical Test with the Ground Water Flow and Cataclinal Slope Simulator

We conducted our test using the ground water flow and cataclinal slope simulator (Figure 4) designed by [5] to simulate a cataclinal slope with upward groundwater seepage. The ground water flow and cataclinal slope simulator consists of an inclinometer platform and a constant-head tank. Three water outlets are evenly distributed from the bottom to the top of the platform. The water flow for each outlet can be adjusted using a valve. The configuration of the ground water flow and cataclinal slope simulator is as shown in Figure 4.

The constant-head tank can provide different water pressures via height adjustments, and the valves can be turned to different angles to control the water flow. In this study, we fixed the angles of the valves so that the water column was not higher than the top of the particle layer. When the valves were open at the same time, the water pressures at the top, middle, and bottom valves were 13.9 kN, 14.5 kN, and 15.5 kN, respectively. When only the top valve was open, the water pressure at the outlet was 17.4 kN. Once the water flows out of the ground water flow and cataclinal slope simulator from the outlets, the water pressure dissipates. The actual water pressure received by the blocky layer is thus lower. In the numerical simulation, the water pressures that were measured were the maximum water pressures.

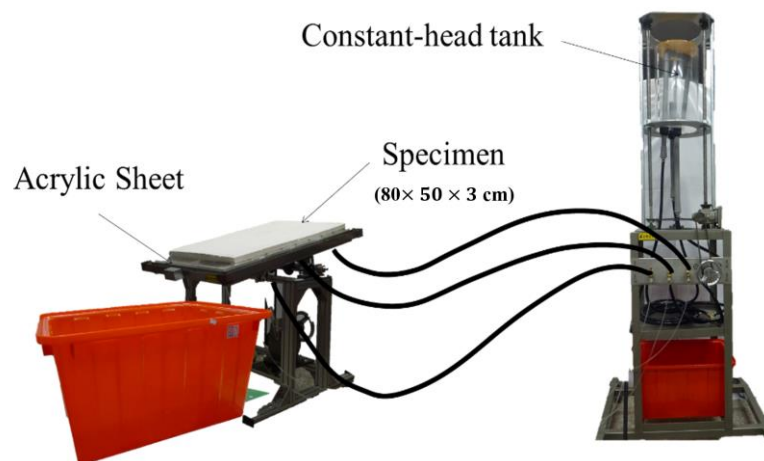


Figure 4. The ground water flow and cataclinal slope simulator.

2.2.1. Material Composition of the Physical Model

According to field surveys, the materials used in physical model included artificial rock spheres (as the uppermost layer of the weathered rock mass), triangular columns (as the middle layer of the sliding rock mass), and gypsum board (as the lowermost layer of bed rock). Then, the study used resin to simulate the adhesion between rock masses. We mixed round artificial rocks that were 1.2 cm in diameter in paste to form a cohesive particle layer that simulated the regolith that declined in strength when soaked in water. The paste comprised glutinous rice flour and water at a ratio of 1:9 to form the weak matrix material of the weathered rock mass. The jointed rock mass in the conceptual model consisted of gypsum board and triangular columns. The length, width, and height measurements of the latter were 3.2 cm, 3.2 cm, and 2.8 cm, respectively. The artificial rock spheres were used to simulate the flexible deformation characteristics of the weathered rock mass or argillite, while the triangular columns were used to simulate the brittle rupture and deformation characteristics of sandstone. Even though the particles of artificial rock were larger than those onsite, their use simplified the simulation of groundwater infiltration and rock porosity. Additionally, the key material that reflects the deformation in cataclinal slope is the resin, which presents the weakening of rock mass when exposed to water. The strength of the solidified resin under dry conditions is 0.79 MPa (shear strength). When the resin is soaked in water, the strength decreases rapidly to approximately 40% of its original value in

20 min, and to 10% in 120 min [6]. Moreover, the shape of the artificial rock can be used to control the failure type of the rock slope model (upper layer belongs to debris slide; lower layer belongs to translational rock slide) and so can reflect the characteristics of rock mass failure type more accurately than other materials.

2.2.2. Test Items and Procedures

During the physical test, we observed and recorded the failure of the specimen as the water flowed upwards from the bottom to understand the factors influencing the locations and types of the failures. We tested: (1) a gradually increasing tilt angle, and (2) a fixed tilt angle in the inclinometer. The objective of the first was to understand the factors that influence where the sliding takes place. After understanding the controlling factors of sliding, we conducted the test with a fixed tilt angle so as to eliminate the influence of vibrations caused by increases in the tilt angle. A video recording was made from the side and the front. The camera at the front moved with the tilt angle during the first test to maintain the perspective (black camera in Figure 5). In the second test, the camera at the front was placed on a tripod as depicted by the red camera in Figure 5. Table 1 presents the conditions of the ground water flow and cataclinal slope simulator, and the contents of the tests were as follows:

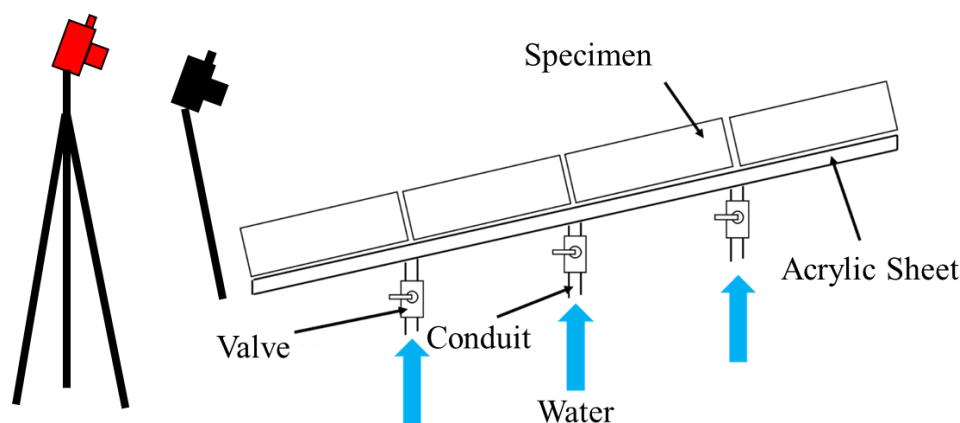


Figure 5. Configuration of the specimen and cameras.

Table 1. Conditions of the physical test.

Model	Tilt Conditions	Composition of the Blocky Layer	Bonding in the Particle Layer	Opened Valves
1	Gradually increasing tilt angle	Gypsum board × 4	No bonding	No seepage
2			Paste	Top, middle, bottom valves
3				Top valve
4				No seepage
5	Tilt angle fixed at 15°	Block of rhombus-shaped grinding stones fastened together with white glue × 2	Paste	Top valve
6		Separated rhombus-shaped grinding stones		

(1) The tilt angle was gradually increased:

To understand the factors and conditions of specimen failure, we controlled water valves so that water flowed from fixed locations, maintained steady water flow, and gradually increased the tilt angle of the inclinometer.

The procedure was as follows:

- a. Gypsum boards and bonded round grinding stones were placed on the level platform. The frame enclosing the grinding stones was removed.
- b. The designated valve(s) was opened.
- c. The tilt angle was gradually increased, the process of specimen failure was observed, and the tilt angle of the platform at the time of failure was recorded.

(2) The tilt angle was fixed (by changing the size of the blocks):

To simulate the interactions between the regolith and the strata at the rock–soil interface during sliding, we used smaller rhombus-shaped grinding stones to form the blocky layer. Furthermore, to reduce the influence of vibrations on specimen stability, we used a fixed tilt angle and observed the failure in the specimens caused by the weakening effect of steady water flow. In Models 5 and 6, the blocky layer comprised rhombus-shaped grinding stones to simulate rock with different joint densities. In Model 5, the rhombus-shaped grinding stones were fastened together in an 8×6 arrangement using white glue and air-dried for over 48 hours, ultimately creating two larger grinding stone blocks. In Model 6, the rhombus-shaped grinding stones were not glued together to simulate a rock mass with a higher joint density. The top valve was open in both Model 5 and Model 6, and the tilt angle was fixed at 15° as the failure process of the specimen was observed (Figure 6).



Figure 6. Schematic of specimen configuration.

The procedure was as follows:

- a. The blocky layer and bonded round grinding stones were placed on the level platform.
- b. The tilt angle of the platform was increased to 15° , and then the frame enclosing the grinding stones was removed.
- c. Approximately 10 minutes were allowed for the particles to reach equilibrium with no water flow.
- d. The designated valve(s) was opened, and the failure caused by water flow was observed.

Use of the physical model to investigate the Zhongzhi landslide case involves several simplified conditions, but this paper is just an initial study in order to explore the failure and slide behavior of cataclinal slopes through the influence of groundwater. Of course, the complex slope failure has many mechanisms involved. These mechanisms are quite difficult to reproduce with a physical model. In the field, there is groundwater seepage from the ground through the joints of rock mass during rainless conditions, as well as cataclinal slope toe daylight. Therefore, based on our field investigation, this study preliminarily selected groundwater seepage with slope toe daylight as major causative factors in order to explore their influence on cataclinal slope slide. For the physical model tests, we had to simplify the field conditions so only the groundwater seepage was considered as a triggering factor. Even though the triggering factors are simple, the simulated results indeed reflect the phenomena of the field investigation, such as the rock mass slide and rock block separation due to groundwater seepage. Though many situations of engineering practice are not considered in the physical modeling,

more triggering factors will be adopted in the future to exhibit more realistic failure characteristics of cataclinal slopes.

2.3. PIV (Particle Image Velocimetry) Analysis

We analyzed the velocities of the round grinding stones using the particle image velocimetry tool PIVlab for Matlab Version 2010–2018 [7] to facilitate our explanation of specimen movement behavior and provide a basis for the settings of our numerical simulation.

PIV is often used to observe the flow fields in fluid mechanics experiments. With non-contact measurements, PIV does not affect the flow field, and by comparing two images taken at short intervals, the velocity field of the entire flow field in a small time interval can be obtained. Aided by PIV, we analyzed the velocities of the round grinding stones at different stages of the physical tests to provide reference for the settings of our numerical simulation.

The analysis process was as follows:

- (1) Fourteen sets of images from different stages of the physical tests were input, each set containing two images taken one second apart.
- (2) A given length and time interval were set for the images for software calibration.
- (3) The region of interest was selected. The region that we chose in this study included the particle layer covering the blocky layer, extending outside of the blocky layer to the distance that the grinding stones may move downslope within a second.
- (4) The interrogation areas, also known as windows, were set. Generally speaking, larger windows mean smaller errors and smaller vector densities within the same range. In the settings, the number of passes can be increased, and by gradually shrinking the windows, vectors of better quality and greater density can be obtained at the same time. However, a greater number of passes also means a longer computation time. In this study, we performed three passes to obtain a reasonable vector field.
- (5) Analysis was conducted.
- (6) Vectors outside seven standard deviations were eliminated; vectors that were obviously unreasonable (vectors with excessively large displacements or point toward higher points in space) were manually eliminated, and points with no data were interpolated.
- (7) Central water flows and regions with more evenly distributed vectors were chosen to calculate the mean velocities on the surface of the particle layer.

2.4. Numerical Simulation of Physical Tests (PFC3D)

PFC3D [8] is a discrete element method software; its advantages include: (1) being able to separate elements, (2) allowing blocks consisting of elements to fail when bearing forces greater than its bonding strength, and (3) consideration of the collision and energy dissipation behavior of materials. It is therefore an appropriate tool to simulate the movements of sliding masses in landslides with large displacements. However, simulating fluid–solid interactions using the discrete element method is currently extremely complex. We therefore used designated materials, different bonding parameters at different stages, and the application of external forces to consider the weakening of specimens as well as the seepage force and water pressure generated.

2.4.1. Material Parameters of the Digital Model

The parameters of the grinding stone elements in the digital models were based on the reasonable parameters obtained by [9,10] in physical test simulations. The adjusted parameters are presented in Table 2.

Table 2. Microscopic parameters of the digital model.

Microscopic Parameters		0 s	0–175 s	175–200 s	200–230 s
Unit weight of ball elements (kg/m ³)		2530			
Friction coefficient of ball elements (particle layer)	Upper section	0.38	0.965 (per 5 s)	0.965 (per 5 s)	0
	Lower section		0.997 (per 5 s)	0.997 (per 5 s)	0
Friction coefficient of ball elements (blocky layer)		0.38	0.85		
Friction coefficient of wall elements		0.4663	0.9		
Normal stiffness (N/m)		1.00 × 10 ⁸			
Shear stiffness (N/m)		4.17 × 10 ⁷			
Normal bond strength (N) and Shear bond strength (N) (contact bond)	Upper section	0.0864	0.965 (per 5 s)	0.965 (per 5 s)	0
	Lower section		0.997 (per 5 s)	0.997 (per 5 s)	0
Force (N)		-	0.0023	0.005	0.007
Normal damping coefficient		0.6	0.5	0.5	0.2
Shear damping coefficient		0.3	0.25	0.25	0.1

2.4.2. Parameter Calibration

Due to the lower strength of the paste in the physical tests, we could not use the normal soil mechanics tests to obtain material strength. We therefore conducted slump–flow tests with a slump cone made of imitation concrete and measured the slump and flow diameter to calibrate the friction coefficients and bonding strength for no-seepage conditions in the numerical simulation. Mechtcherine et al. [11] compiled various applications of DEM (Discrete Element Method) to simulate slump–flow tests for fresh concrete. The earliest relevant simulations were performed using PFC (Chu and Machida [12], Petersson and Hakami [13], Schwabe and Kuch [14], and Shyshko and Mechtcherine [15]). The final appearances of the specimens were used to verify the reasonableness of the parameters. The particle layer in our physical tests flow in a way that is similar to that of fresh concrete. Thus, we also used PFC to perform the simulations. The simulation results were then compared to those of the actual tests to calibrate the parameters used in the subsequent ground water flow and cataclinal slope simulator test simulations.

The slump cone used in the slump–flow tests was 100 mm in top diameter, 200 mm in base diameter, and 300 mm in height. The specimen comprised round grinding stones mixed with paste of the same mixture ratio as that in the ground water flow and cataclinal slope simulator tests (comprising grinding stones 7240 g, glutinous rice flour 151.1 g, and water 1360 mL). It was tamped in three layers, and once complete, we recorded the process from cone mold removal to the specimen reaching stability. The cone mold was removed vertically at a fixed velocity, the process taking approximately 4 s. The period from cone removal to the specimen reaching stability was roughly 110 s. Once the specimen reached stability, we measured the flow diameter and the vertical distance between the top of the cone mold and the center of the slumped specimen (Figure 7).

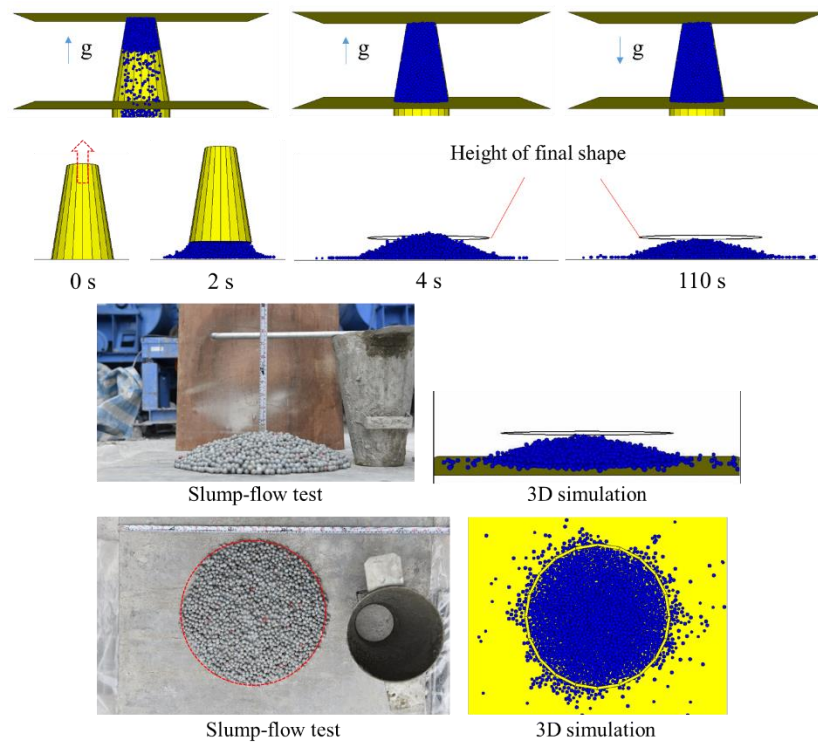


Figure 7. Results of slump-flow test and numerical simulation.

2.4.3. Influence of Water Flow

The adverse influences of groundwater on slopes include: (1) applying water pressure to vertical cracks (joints or tension cracks), which push rock or soil slopes downwards, (2) applying uplift forces to potential sliding surfaces, which reduces the shear resistance in said surface, (3) lubricating sheet-like minerals (particularly clay minerals), (4) dissolving the cementing materials in sandstone, and (5) applying other physical and chemical forces that reduce the mechanical strength of the rock or soil [16].

The numerical simulation in this study showed that the water flow reduced the friction coefficients of the elements, weakened bonding strength, applied seepage force to the particle layer, and applied uplift and lateral force to the blocky layer (Figure 8). The reduction of friction coefficients and bonding strength was based on the downward velocity of the particle layer during the experiment and was divided into various stages of weakening, thereby gradually decreasing the microscopic parameters. For the seepage and lateral forces, we measured the height of the water table during the tests and then adjusted the microscopic parameters based on the simulation results after calculations. Figure 7 displays the relevant configurations.

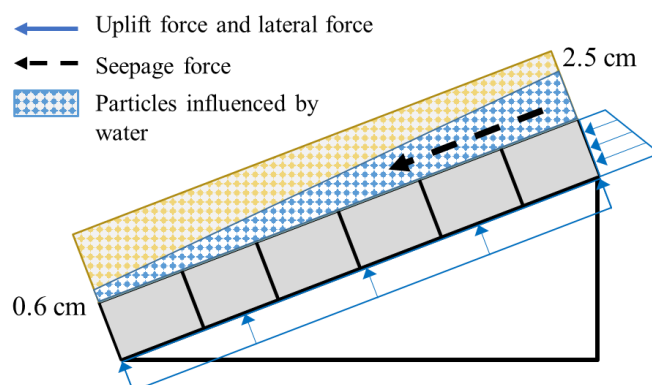


Figure 8. Schematics of water flow influence.

2.5. Numerical Simulation of the Field Case (PFC3D)

We constructed a full-scale model of the Zhongzhi landslide using PFC3D. The dimensions and coordinates of the original terrain came from the digital surface model (DSM) created by the UAV (Unmanned Aerial Vehicle) after Typhoon Soudelor (24 September 2015). The range of the landslide simulation principally comprised the exposed landslide area. After the landslide, little vegetation remained on the movement path. We considered this the ground surface and compared it against a digital $5\text{ m} \times 5\text{ m}$ DEM from 2008. We established the wall elements in the digital model by subtracting the deposit heights from the post-landslide terrain, using the post-landslide terrain for the source zone and transportation zone of the landslide, and using the pre-landslide terrain for the deposition zone.

The sliding mass was simulated using ball elements, and the range of the mass was mapped based on an orthophoto. The entire landslide area was divided into a source zone, an uphill transportation zone, the midstream Zhongzhi cataclinal slope, and a downhill transportation zone based on similarities in lithography and estimated sliding mass thickness. Elevation differences between field investigation measurements and digital terrain models served as reference for landslide depth. The estimation of sliding mass thickness, the selection of material parameters, and the water pressure settings are explained in this section.

2.5.1. Microscopic Parameters of Materials

For the stratum parameters, we referred to the results of the physical property tests and uniaxial compression tests on drilling samples taken by CECI Engineering Consultants, Inc., Taipei City, Taiwan from the slopes over 10.2 K on Provincial Highway No. 9A. Uniaxial compression tests were simulated using PFC3D. To convert the macroscopic parameters into microscopic parameters, we first converted the uniaxial compression results and the Young's modulus using the conversion formula suggested by Potyondy [17], and then made adjustments until the simulation results corresponded with the actual uniaxial compression test results. In this manner, we derived reference values for the microscopic parameters of the ball elements in the digital model, including the normal and shear stiffness of the ball elements, the normal and shear strength and stiffness of the parallel bonds, and the friction coefficients of the ball elements. For the unit weights of the colluvium and regolith, we also referred to the physical test results derived by CECI Engineering Consultants, Inc., Taipei City, Taiwan. However, there were no data from relevant mechanics tests, so we used reduced rock parameters for the microscopic parameters of the materials.

For the damping parameter that controls the dissipation of energy during material collisions in PFC, we employed the critical damping ratio that Lo [9] derived from the suggested rebound coefficients of different geological materials [18]. For the rock layer, we used a normal damping ratio

of 0.32 and a shear damping ratio of 0.05, whereas for the regolith, we used normal a damping ratio of 0.36 and a shear damping ratio of 0.11.

Limited by available computational resources, we set the diameters of the particles in the full-scale model at 3 m. Based on the magnification rate of ball element radius, we referred to Tsai [19] and compared centrifuge test results and numerical simulation results to revise the dimensional conversion relationships of the PFC microscopic material parameters, where the correction factor was 0.3. Then, we performed the dimensional conversion of the uniaxial test parameters to obtain the preliminary parameters of the 3-m ball particles before making adjustments based on the verification items. Table 3 presents the parameters used in the full-scale numerical simulation. Rock parameters were used for the jointed rock in the cataclinal slope, the rock in the source zone, and the sliding mass uphill of the cataclinal slope. Regolith parameters were used for the regolith on the cataclinal slope and the sliding mass downhill.

Table 3. Parameters of field case simulations.

Title	Uniaxial Compression Test	Rock	Regolith
Diameter of ball elements (m)	0.015	1.5	1.5
Unit weight of ball elements (kg/m^3)	2700	2700	2000
Normal stiffness (N/m)	4.26×10^{10}	1.70×10^{11}	2.83×10^{10}
Shear stiffness (N/m)	1.78×10^{10}	7.07×10^{10}	1.18×10^{10}
Friction coefficient of ball elements	0.5	0.5	0.375
Normal stiffness of parallel bond (N/m^3)	6.60×10^{10}	1.66×10^{10}	
Shear stiffness of parallel bond (N/m^3)	3.00×10^{10}	7.54×10^9	
Normal strength of parallel bond (Pa)	7.20×10^7	7.20×10^7	
Shear strength of parallel bond (Pa)	7.20×10^7	7.20×10^7	
Normal critical damping ratio	0.32		0.36
Shear critical damping ratio	0.05	0.05	0.11

2.5.2. Influence of Groundwater

Considering the influence of static water pressure, we applied an upward external force to the ball elements to express the influence of buoyancy on saturated soil and the water pressure applied to the rock mass (Figure 9). As a rising water table increases the seepage pressure in the sliding mass, we referred to the method proposed by Su [20] in which seepage pressure is applied to simulate the movements of a seepage-driven sliding mass under the influence of rainfall. The relevant assumptions and methods of seepage force application are as follows.

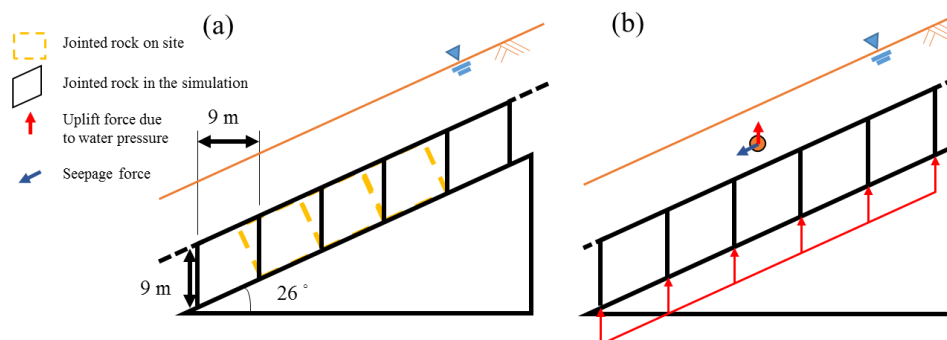


Figure 9. Schematics of (a) the digital model; (b) water pressure settings.

Relevant assumptions of seepage force:

- (1) The water table runs parallel to the slope surface.
- (2) The direction of seepage force runs along the slope surface and parallel to the slope surface.
- (3) The direction of maximum elevation difference is the direction of groundwater seepage.

- (4) Ball elements in the same seepage zone are subject to seepage forces of identical direction and magnitude (Figure 10).

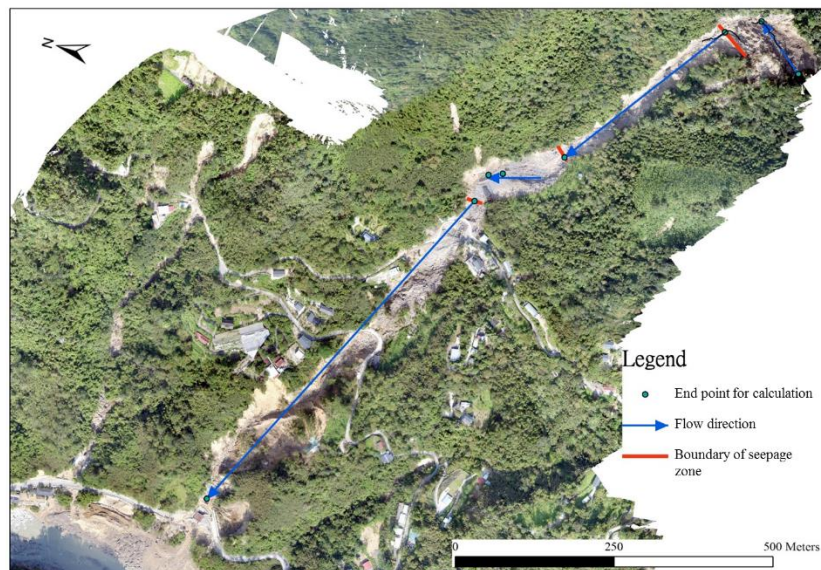


Figure 10. Seepage zones and directions.

Calculation of seepage force:

This study used the concept of the hydraulic gradient to calculate the seepage force per unit volume as $S = i\gamma_w$, where the hydraulic gradient i = the difference between the uphill and downhill hydraulic heads/distance. S is then multiplied by the volume of a single ball element V_{particle} to calculate the seepage force exerted on each ball $F = S \times V_{\text{particle}}$. Using ArcGIS, we depicted a line segment along the assumed direction of seepage, derived the elevations at the two ends, and measured the horizontal linear difference between the two points to calculate the hydraulic gradient and unit seepage force for seepage force calculation in PFC3D.

In reality, the water table in a slope rises and falls depending on the precipitation. Su [20] examined different water tables to assess their influence on the movement of sliding masses. The results indicated that the water table only influences whether the sliding mass moves but has a limited influence on simulation results. We therefore set the seepage force to disappear once displacement reached five times the radius of the ball elements and experimented with two conditions in our simulations: (1) a water table identical to the ground surface, and (2) a sliding mass containing no groundwater. The purpose of these experiments was to evaluate the feasibility of applying seepage force to trigger landslides.

3. Results

3.1. Physical Tests

3.1.1. Gradually Increasing Tilt Angle

The toe of a cohesive particle layer slope lacks support, as is the case in a daylight cataclinal slope. When the top valve is open so that water flows from the bottom of the ground water flow and cataclinal slope simulator, the bonds in the particle layer are weakened, and the particle layer gradually slides downhill (as the water seeps from the middle of the profile, we describe the central area with greater water flow). When the top, middle, and bottom valves are open at the same time, the time to the complete collapse of the particle layer is shortened. The water flow below the middle valve is greater than that above the middle valve, so the bonds below the middle valve weaken more quickly,

as shown in Figure 11. During the test, we can observe that different sliding velocities in the two parts of the slope result in a depression in the middle. The test results indicate that soaking weakens the slope materials and that the flow rate is a crucial factor of whether and how fast the slope fails.

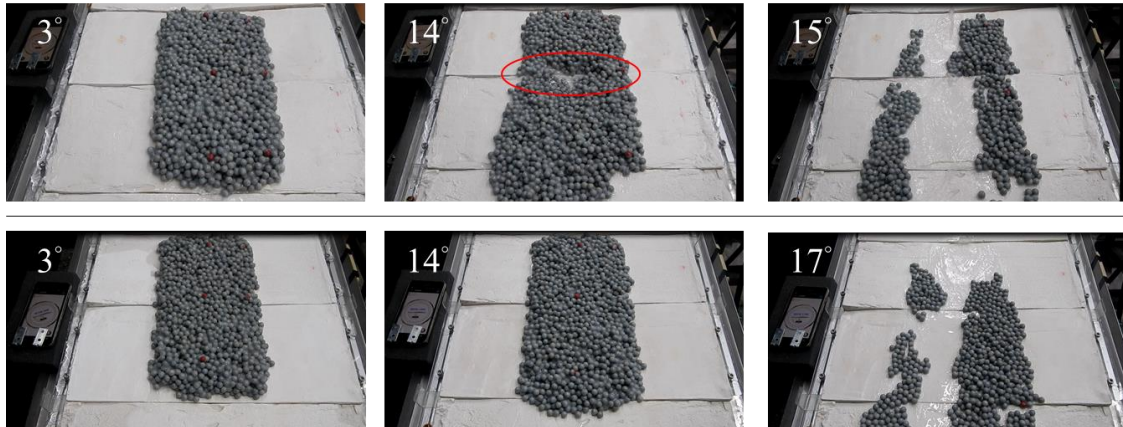


Figure 11. Results of Model 2 (top; top, middle, bottom valves open) and Model 3 (bottom; top valve open).

3.1.2. Fixed Tilt Angle

When the blocky layer comprises rhombus-shaped grinding stones, the failure also begins in the particle layer, and the cause can be observed. When the blocky layer consists of the two larger grinding stones (Model 5), no sliding occurs between the blocky layer and the platform. However, when the blocky layer is more fragmented (Model 6), the bottom blocky grinding stones will begin to slip after the top particles completely slide out of the bottom blocky grinding stones, as shown in Figure 12. This supports the notion that the degree of rock fragmentation in the slope (or density of joint distribution) is a crucial factor determining whether the rock mass will slide.

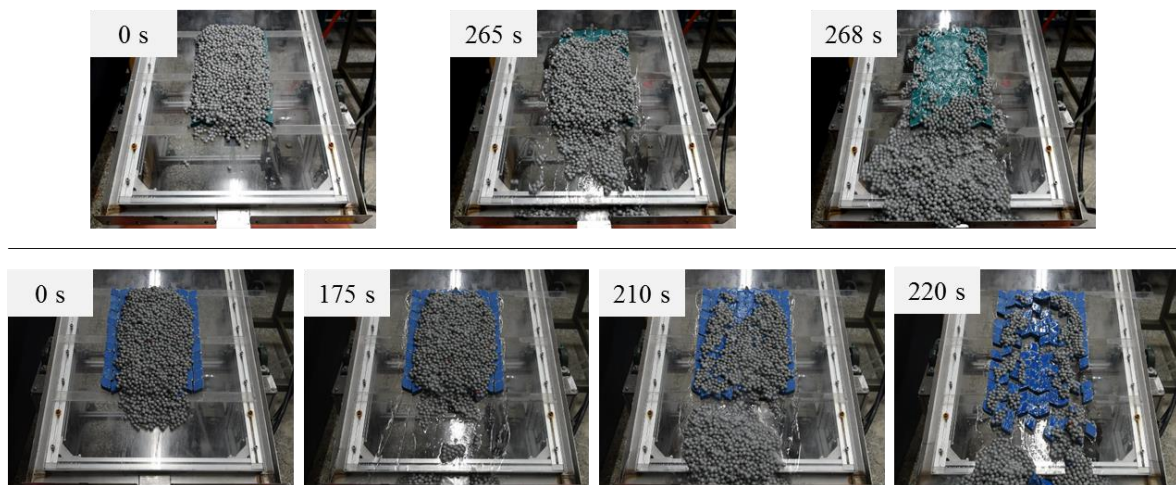


Figure 12. Model 5 (top): blocky layer bonded into two larger specimens. Model 6 (bottom): grinding stones in blocky layer not bonded together.

3.2. PIV Analysis Results

Figure 13 shows the PIV analysis results of velocity fields at different stages. The specimens were arranged to imitate cataclinal slopes, so we took note of the velocity component v , which is parallel to the aspect of the slope, and mainly examined the movement behavior in the center of the slope where

the water flow is more uniform. We used the red box shown in Figure 13 to calculate the mean velocity and plotted the relationship between mean velocity and time in Figure 14. The velocity curve shows a turning point at approximately 175 s after the valve is turned on. Based on the image records and PIV analysis results, we observed the following movement behavior in the particle layer:

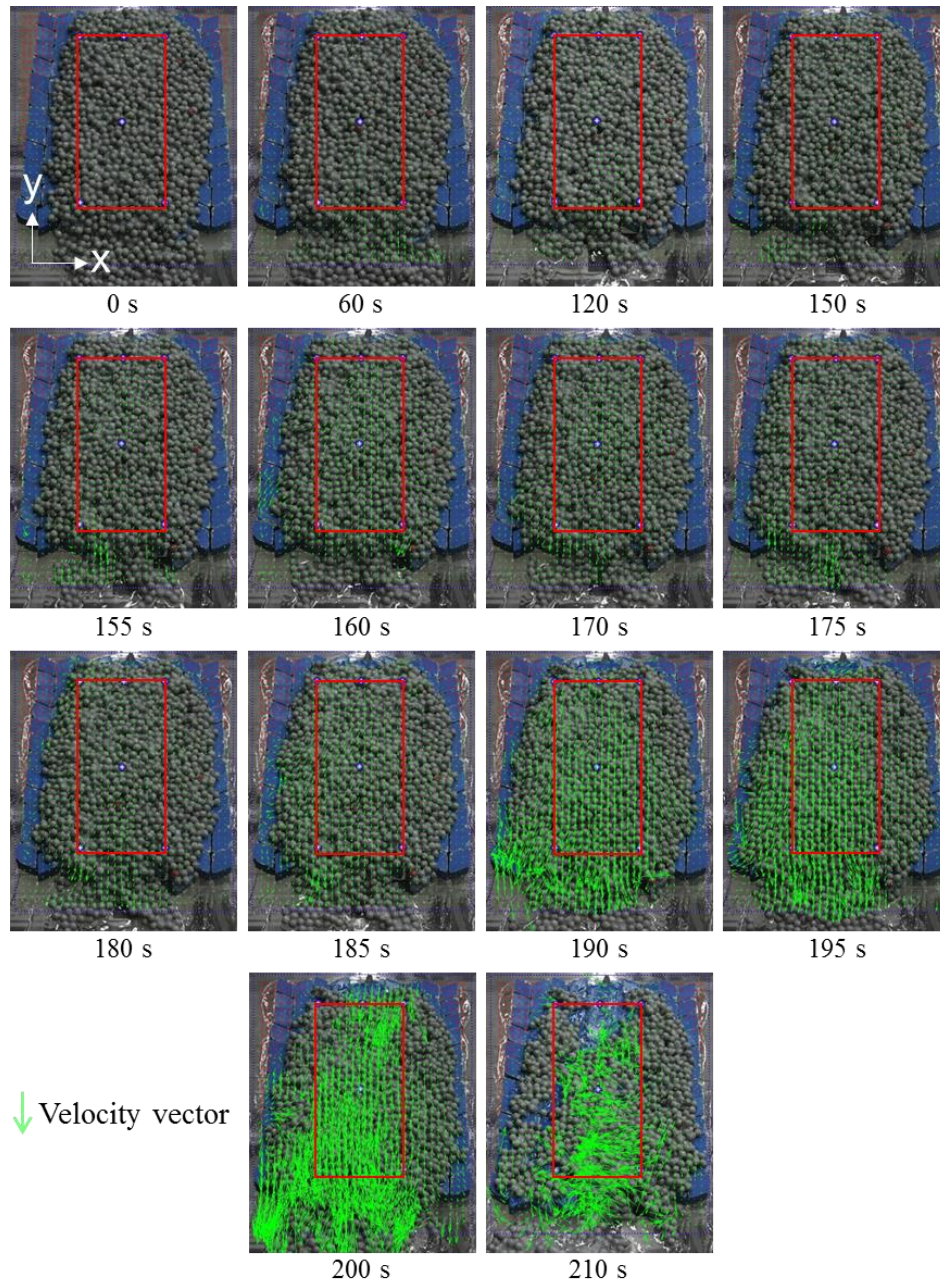


Figure 13. Velocity fields of round grinding stones at different stages.

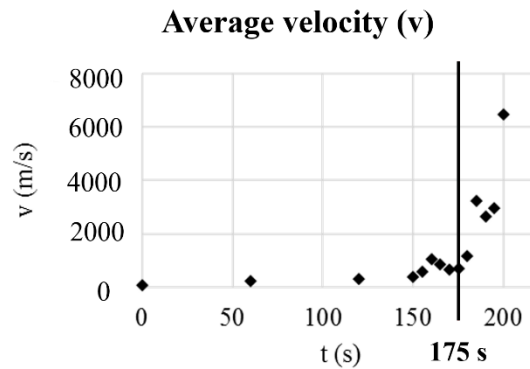


Figure 14. Average velocity of grinding stones in the top layer.

- (1) 0 s: With the valve closed, the tilt angle was increased to 15 degrees and the frame enclosing the grinding stones was removed. Gravity prompted the particle layer to spread laterally and deform slowly downwards. Once the particle layer stabilized with no water flow, the velocity vectors in the PIV analysis results also approached zero.
- (2) 0 s~60 s: Once the specimen reached stability in the previous stage, the valve was turned on. Water gradually flowed into the particle layer, weakening it and causing it to deform downwards like a slope with a cut toe. Figure 13 shows velocity vectors beginning to appear at the toe in the PIV results.
- (3) 60 s~150 s: The toe of the particle layer continued to move downwards. At 120 s, the toe particles came into contact with the acrylic sheet and were largely separated from the main body of the layer. The bonding materials gradually weakened with time. The passive earth pressure applied to the upper particles gradually decreased, and the particles gradually loosened. The range of appearing velocity vectors spread up the slope, and the velocity vectors within the particle layer became increasingly apparent, like the progressive failure in an actual slope. At approximately 150 s, all of the particles in the red box presented downward velocities.
- (4) 150 s~175 s: During this stage, the central parts of the particle layer where the water flow was adequate were all moving down the slope. The mean velocity of the surface particles in the red box was slowly and steadily beginning to rise.
- (5) 175 s~200 s: The velocity vectors in the PIV images revealed significantly greater velocities, and the velocity–time curve presented a substantially steeper slope. The mean velocity during this stage was roughly 11 times that of the mean velocity during the period 0 s~150 s. The velocity field distributions show that round grinding stones with increasing velocity in the center where the water flow is adequate as well as greater displacements than those of the grinding stones on both sides. The top of the particle layer also presented a depression created by differences in displacement.
- (6) 200 s~220 s: During this stage, the particle layer continued to accelerate downwards; the central part where the water flow was adequate ultimately separated from the blocky layer completely. Here, the particles presented significant movement velocities that were difficult to analyze, so we did not include the mean velocity of this stage in our comparison.

According to the PIV analysis above, the subsequent numerical simulation could be divided into four stages based on the mean velocity: the stage before the valve is opened and the three stages after the valve is opened (0 s~175 s, 175 s~200 s, and 200 s~220 s). These stages serve as reference for microscopic parameter adjustments in the digital models.

3.3. Results of Physical Test Simulations

With the parameter settings of no water flow in the numerical simulation, the particle layer slowly deformed due to gravity, stabilized, and then stilled. A comparison of the particle layer in this stage revealed an appearance similar to that of the physical test. However, a comparison of the front view still showed that the numerical simulation could not present the same deposition behavior in the particles sliding onto the platform as that in the physical test. Rather, the particles continued to move downslope. We speculate that this is because the energy dissipation behavior between wall elements and ball elements in PFC is inconsistent with reality. However, this study focused on the center of the blocky layer where the water flow is uniform, so we do not discuss this further.

Next, we reproduce the conditions observed in the physical test during different stages after the valve was opened. In the models of the numerical simulations, the water flow weakened the center of the particle layer in three stages (parameters as shown in Table 2), and a uniform and stable seepage force was applied to the region of interest.

The simulation results (Figure 15) successfully presented the weakening of bonds, the decrease in the friction coefficient and the seepage force, and the downward movement of the particles. The specimens weakened more quickly where the water flow was adequate and therefore presented greater downward velocities. The simulation results for the stage from 0 s to 200 s were similar to the deformation results in the ground water flow and cataclinal slope simulator tests. After 200 s, the velocities in the particle layer in the numerical simulation were still inconsistent with those in the physical tests. We therefore speculate that the damping settings require further adjustment. Furthermore, as we could not accurately measure the water table, water pressure, and the weakening rate of the bonding materials in the physical tests, the numerical simulations were not consistent with the results of the actual tests. Nevertheless, this study succeeds in demonstrating the influence of water flow on specimens in PFC. Specific description of relevant hydraulic conditions would enable simulations of higher accuracy.

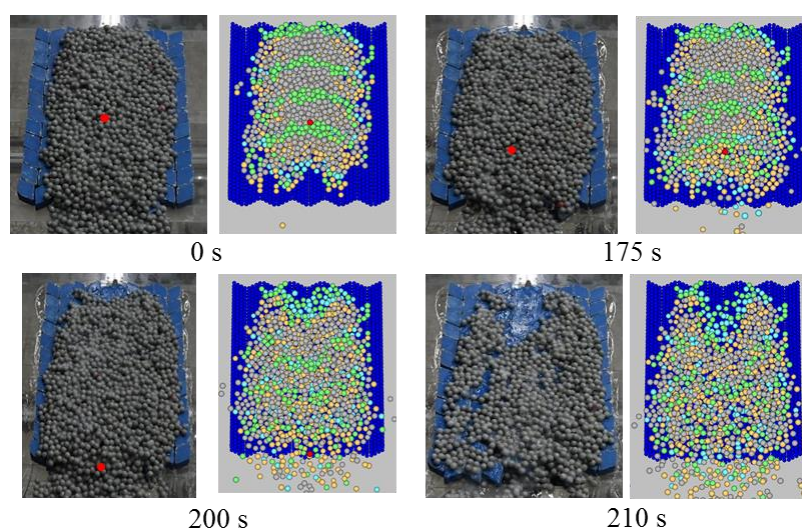


Figure 15. Comparison of physical tests and digital model.

3.4. Material Composition of the Physical Model

3.4.1. Results of Field Case Simulations

To verify the results of the numerical simulations, we compared the simulation results against onsite conditions. There were several key points of comparison. Firstly, the jointed rock mass and regolith that originally covered the cataclinal slope should move in a landslide event. Secondly, many new rocks were deposited near 10.2 K of Provincial Highway No. 9A in the landslide area after

Typhoon Soudelor, and most of the strata exposed downhill of the landslide area were colluvium. Thus, it is speculated that the rocks were argillite from the Zhongzhi landslide. Some rock deposits were also found in the midstream and downhill portions of the Zhongzhi landslide. Thus, the rock of the cataclinal slope should reach the river channel of the Nanshi River in the simulation, and some of the uphill materials should remain in the midstream and downhill parts of the river (Figure 16). Thirdly, the majority of the rocks deposited in the river channel were smaller than 4 m, so the jointed rock should shatter during the landslide process in the simulation.



Figure 16. Landslide deposition area.

3.4.2. The Simulated Landslide Process

We first used the results of indoor uniaxial compression tests to convert the macroscopic parameters into microscopic parameters. Based on the aforementioned key points of the comparison, we then searched for reasonable microscopic parameters. The Zhongzhi landslide was the result of rainfall infiltration reducing the effective stress in the landslide mass, which then caused the joint-filled rock uphill and the colluvial material downhill to slide. The reduced friction coefficient and the influence of water pressure and seepage force triggered the landslide. After parameter calibration, we found that the simulation results from bond strength 4×10^7 , rock ball friction coefficient 0.3, regolith ball friction efficient 0.075, and wall friction coefficient 0.2 were the most consistent with the deposits created by Typhoon Soudelor and the sliding sequence derived from the physical tests. The results of the physical tests indicate that if the failure in a cataclinal slope covered by both the blocky layer and the particle layer begins at the bottom of the blocky layer, then the shear strength of the interface between the blocky layer and the bottom surface will be lower than the bonding strength of the particle layer. In the Zhongzhi landslide, the cataclinal slope of focus was situated on a more complete argillite residual slope that was originally covered by jointed rock and the regolith. The strength and friction angle of the rock was greater than those of the regolith, so failure and sliding should supposedly begin in the regolith.

From uphill to downhill, the ball elements in the PFC digital model of the Zhongzhi landslide can mainly be divided into five sliding masses based on thickness and material, which are A: the source zone material, B: the uphill transportation zone material, C: the jointed rock, D: the regolith of the cataclinal slope, and E: the downhill transportation zone material. The simulated landslide process took approximately 2400 s (Figure 17) in total. Figure 18 displays an enlarged view of the cataclinal slope and the sliding sequence of the jointed rock and regolith. Before the landslide is triggered, the regolith is evenly distributed on the jointed rock. Once the ball elements are impelled to move, all of the sliding masses begin to slide. At 10 s, it is clear that the regolith slides further than the jointed rock underneath it; the regolith layer is thicker at the turning point at the toe of the cataclinal slope than it is uphill, and some of the regolith particles have already surpassed the front end of the jointed rock,

which means that the regolith presents greater displacement. At the turning point of the cataclinal slope, the particles hit a rock wall, slow down, and then continue sliding downhill from the opening at the slope toe. The jointed rock only shows significant bond breaking when it hits the rock wall at the turning point of the cataclinal slope, which indicates the fragmentation of the jointed rock. At 20 s, the materials deposited downhill of the toe of the cataclinal slope have already departed, thereby leaving the cataclinal slope with a cut toe. Thus, the fragmented jointed rock at the slope toe as well as the regolith continue sliding downwards. Between 40 s and 90 s, the jointed rock is squeezed by mass B and continues to break up and slide downwards. The unbroken jointed rock slows down and lingers temporarily at the turning point of the cataclinal slope. Between 90 s and 120 s, mass A reaches the cataclinal slope, impacting masses C and B that linger here. All three masses then continued sliding downwards. From 120 s to 330 s, some of the material in mass E decelerates. However, at this point mass C, which was originally located uphill of mass E, reaches the downhill transportation zone and scours the material deposited there, which prompts the originally decelerating colluvium to continue downhill. Mass E is then transported to the channel of the Nanshi River during this stage. Between 210 s and 900 s, the curve of the erosion gully causes masses C, B, and A to slow down in that order, and the masses uphill mix with those downhill. The continued transportation downward is also due to the bend in the river channel, which dissipates the energy of the materials in masses A, B, and B and slows them down. Some of the debris is thus deposited midstream where the erosion gully is narrower. When the numerical simulation reaches equilibrium, we can see that some of the materials are distributed in the midstream portion of the river channel (downhill of the cataclinal slope), which is consistent with some of the rocks deposited onsite. The sliding masses transported to the Nanshi River then form a fan-shaped deposit and compress the channel of the Nanshi River.

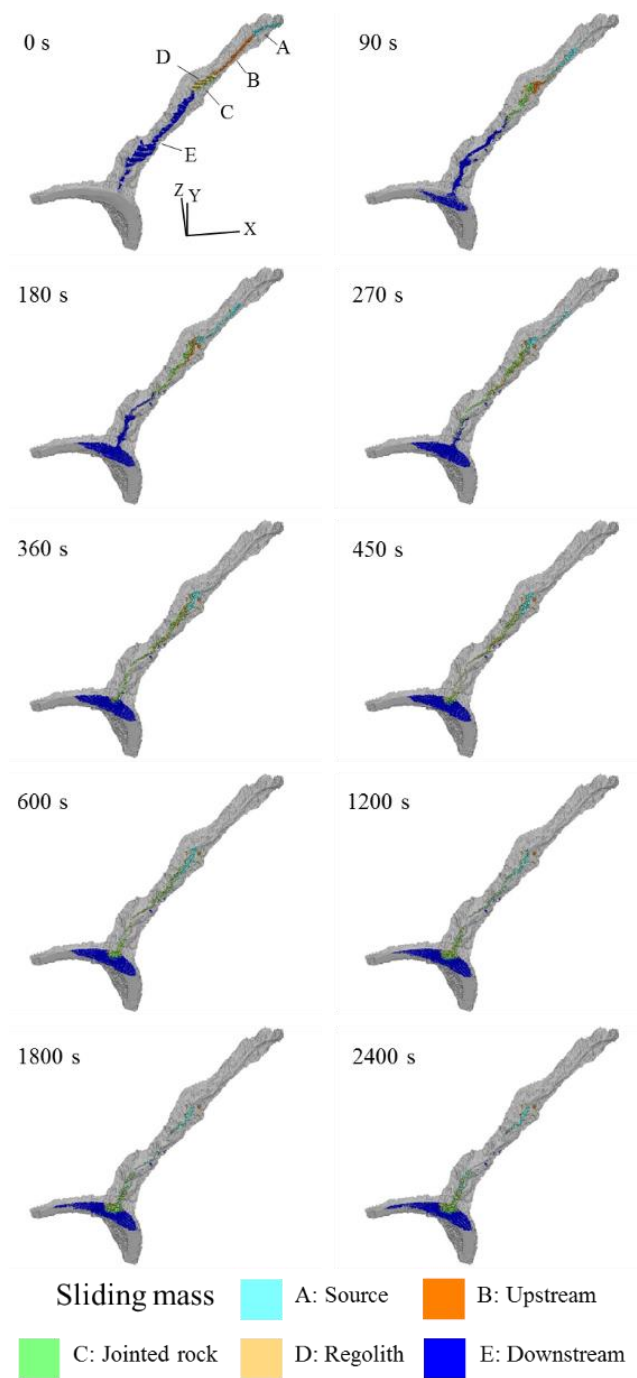


Figure 17. Results of the Zhongzhi landslide simulation.

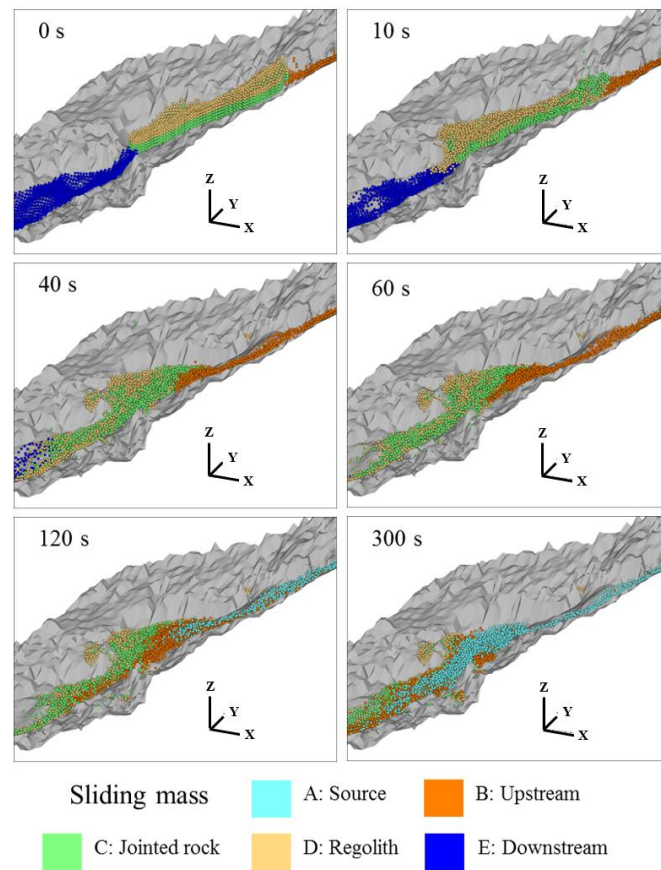


Figure 18. Simulation of the cataclinal slope during landslide.

The numerical simulation in this study does not consider the scouring effect of the river water on the bed of the Nanshi River, so it is expected that the simulation results will differ somewhat from the actual deposit in appearance. Nevertheless, the deposition sequence will remain the same. Furthermore, with field investigations and orthophoto interpretation, we can determine the range of the fan-shaped deposit created by the Zhongzhi landslide based on the larger rocks deposited in the river channel. Figure 19 compares the deposition zone on an orthophoto and that resulting from our numerical simulations, with an error of approximately 1% in area. In the numerical simulations, we can still observe that the deposition sequence is associated with the sliding sequence. The regolith of the cataclinal slope ended up closer to the front and bottom of the fan-shaped deposit, which means that the regolith began sliding first and reached the channel of the Nanshi River first. The simulation of the Zhongzhi extends in the physical tests and their simulations; the sliding conditions of the cataclinal slope are consistent: the failure initially began in the regolith, and then the materials in the downhill transportation zone of the cataclinal slope collapsed and led to daylighting, thereby causing the regolith and the jointed rock with a fragmented toe to slide downwards. This was different from the physical tests, which simply simulated a cataclinal slope with large displacements only in the upper layer of materials (the particle layer). When the uphill sliding masses in the numerical simulation passed masses C and D, they collided with and scoured the jointed rock. This caused the jointed rock, which originally had only moved slightly, to continue sliding down the slope.

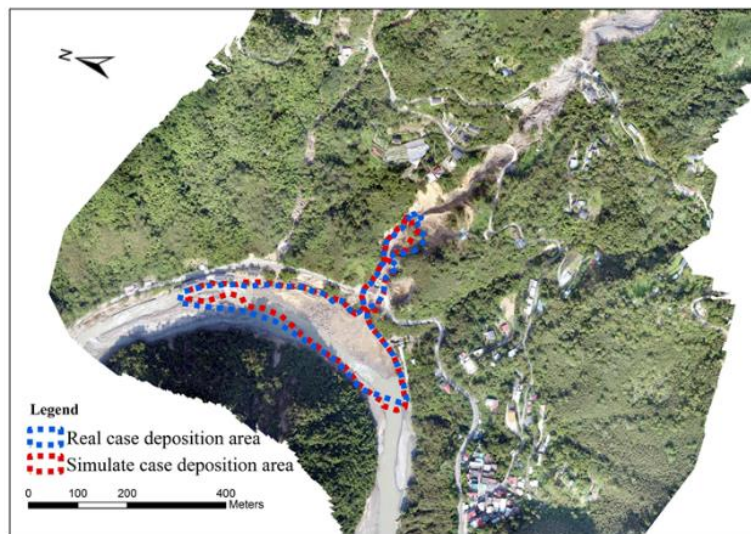


Figure 19. Ranges of deposits onsite and in numerical simulation.

4. Conclusions

This study utilized the ground water flow and cataclinal slope simulator to investigate the factors that influence the location of the initial sliding surface in cataclinal slopes with groundwater seeping upwards. We then attempted to display the influence of water flow on specimens in PFC3D and simulated the Zhongzhi landslide, which was triggered by heavy rainfall. The results indicate that the friction angles of different stratum interfaces, the strength of the strata, the degree of fragmentation in the materials, and whether soaking the materials weakens them are all crucial factors that determine where the sliding surface appears.

The results of the physical tests and digital models show that water flow affects slope stability by weakening bond strength, reducing friction angles, and applying lateral, uplift, and seepage forces which are not conducive to stability.

The digital models successfully present the influence of water flow on displacement in the particle layer in the ground water flow and cataclinal slope simulator experiments via the weakening of designated bonds and the timing and degree of friction coefficient reduction and give magnitudes of water pressure. Determining the range of water flow influence and the magnitude of water pressure is crucial in numerical simulations. If we could measure the water table and water pressure in the particle layer and the rate at which bonding materials weaken when soaked in the ground water flow and cataclinal slope simulator experiments, we could perform the simulations more accurately.

The numerical simulation of the Zhongzhi landslide revealed that it was triggered by reduced material friction coefficients, the application of seepage and buoyancy forces on soil beneath the water table, and the uplift force caused by water pressure on the rock. The numerical simulation also furthered understanding of the movement behavior of sliding masses in different areas and the interactions among them, and we could make speculations on the landslide process based on the process and deposits in the simulation. Compared to methods that simply reduce the friction coefficients to trigger landslides, our numerical simulation was closer to reality in that a rising water table triggered the landslide.

Author Contributions: Conceptualization, C.-H.W. and M.-L.L.; Methodology, C.-H.W. and C.-M.L.; Software, C.-H.W. and C.-M.L.; Validation, C.-H.W. and C.-M.L.; Formal Analysis, C.-H.W., M.-L.L., and H.-H.L.; Investigation, C.-H.W., M.-L.L., C.-M.L. and H.-H.L.; Resources, C.-M.L. and H.-H.L.; Data Curation, C.-H.W., M.-L.L., and C.-M.L.; Writing-Original Draft Preparation, C.-H.W. and C.-M.L.; Writing-Review & Editing, C.-M.L.; Visualization, C.-H.W. and M.-L.L.; Supervision, M.-L.L. and C.-M.L.; Project Administration, M.-L.L. and C.-M.L.

Funding: This research received no external funding.

Acknowledgments: The research is supported by the Ministry of Science and Technology of Taiwan, Grant no. MOST 106-2625-M-239-004. The advice, comments, and help provided by the editor and two anonymous reviewers have significantly strengthened the scientific soundness of this paper. Their kind efforts are gratefully acknowledged.

Conflicts of Interest: The authors declare no conflict of interest.

References

1. Lin, H.H.; Jih, T.J.; Fei, L.Y. Geo-hazards caused by Typhoon Soudelor in Nanshi River and Pingkong River of New Taipei City. *Geology* **2015**, *3*, 18–21.
2. Wyllie, D.C.; Mah, C. *Rock Slope Engineering*; CRC Press: Boca Raton, FL, USA, 2004.
3. Chan, P.C.; Lin, M.L.; Chang, K.J. Characteristics and scale effect of joint roughness coefficient on failure planes of consequent bedding-parallel rock slopes. *J. Chin. Inst. Civ. Hydraul. Eng.* **2016**, *28*, 129–137.
4. Wei, L.W.; Huang, W.K.; Huang, C.M.; Lee, C.F.; Lin, S.C.; Chi, C.C. The mechanism of landslides caused by Typhoon soudelor in northern Taiwan. *J. Chin. Soil Water Conserv.* **2015**, *46*, 223–232.
5. Huang, S.C. The Influence of Joints with Upward Groundwater on Dip Slope Stability. Master's Thesis, National Taiwan University, Taipei, Taiwan, 2015.
6. Lo, C.M.; Weng, M.C. Identification of deformation and failure characteristics in cataclinal slopes using physical modeling. *Landslides* **2017**, *14*, 499–515. [[CrossRef](#)]
7. Thielicke, W.; Stamhuis, E. PIVlab-Time resolved digital particle image velocimetry tool for MATLAB. *J. Open Res. Softw.* **2014**. [[CrossRef](#)]
8. Itasca. *The PFC3D User's Manual*; Version 3.0; Itasca Consulting Group Inc.: Minneapolis, MN, USA, 2003.
9. Lo, C.M. Cliff Recession and Talus Deposition Pattern in Rockfall Area. Ph.D. Thesis, National Taiwan University, Taipei, Taiwan, 2009.
10. Chuang, T.F. A Study on the Deformational Mechanism of Slate Slopes Using Discrete Element Method. Master's Thesis, National University of Kaohsiung, Kaohsiung, Taiwan, 2014.
11. Mechtcherine, V.; Gram, A.; Krenzer, K.; Schwabe, J.-H.; Shyshko, S.; Roussel, N. Simulation of fresh concrete flow using Discrete Element Method (DEM): theory and applications. *Mater. Struct.* **2014**, *47*, 615–630. [[CrossRef](#)]
12. Chu, H.; Machida, A. Numerical simulation of fluidity behavior of fresh concrete by 2D distinct element method. *Trans. Jpn. Concr. Inst.* **1996**, *26*, 23–30.
13. Petersson, Ö. Simulation of SCC—Laboratory Experiments and Numerical Modeling of Slump Flow and L-box Tests. Available online: https://www.rilem.net/gene/main.php?base=500218&id_publication=38&id_papier=4195 (accessed on 20 August 2018).
14. Schwabe, J.; Kuch, H. Development and control of concrete mix processing procedures. In Proceedings of the 18th BIBM international congress and exhibition, Amsterdam, The Netherlands, 11–14 May 2005.
15. Shyshko, S.; Mechtcherine, V. *Virtual Concrete Laboratory—Continuous Numerical Modelling of Concrete from Fresh to the Hardened State*; Advances in Construction Materials 2007; Springer: Berlin, Germany, 2007.
16. Hung, J.J. *An Outline of Elementary Engineering Geology*; Sino-Geotechnics Research and Development Foundation: Taipei, Taiwan, 2007.
17. Potyondy, D.; Cundall, P. A bonded-particle model for rock. *Int. J. Rock Mech. Min. Sci.* **2004**, *41*, 1329–1364. [[CrossRef](#)]
18. Giani, G.P. *Rock Slope Stability Analysis*; CRC Press: Boca Raton, FL, USA, 1992.
19. Tsai, S.J. A study of Scale Effect on Dip-Slope Deformation Using Centrifuge Test and Distinct Element Method. Master's Thesis, National Taiwan University, Taipei, Taiwan, 2016.
20. Su, H.K. Reconstruction of Rainfall-induced Landslide Dam by Numerical Simulation—The Barrier Lake in Taimali River as an Example. Master's Thesis, National Chiao Tung University, Hsinchu, Taiwan, 2012.

